

# NHR-85 modulates mitochondrial and lipid homeostasis to protect against $\alpha$ -synuclein aggregation in *C. elegans*

Dikaia Tsagkari<sup>1,2</sup>, Maria Markaki<sup>1</sup> and Nektarios Tavernarakis<sup>1,2,\*</sup>

## ABSTRACT

Peroxisome proliferator-activated receptors (PPARs), such as PPAR $\delta$ , are transcription factors that play a pivotal role in energy and fat metabolism. PPAR $\delta$  activates genes involved in lipid and glucose metabolism and is expressed in various human tissues, including all brain regions and especially neurons, where it regulates lipid homeostasis and contributes to neuroprotection. However, the precise molecular mechanisms underlying these protective effects remain poorly understood. Here, we identify the *Caenorhabditis elegans* nuclear hormone receptor NHR-85 as a putative orthologue of human PPAR $\delta$ . Furthermore, we show that NHR-85 functions as an essential regulator of fat and energy metabolism, with significant impact on mitochondrial homeostasis, at least in part through modulation of mitophagy. Finally, we find that NHR-85 prevents  $\alpha$ -synuclein aggregation in a nematode model of Parkinson's disease, suggesting that it might play a protective role in neurodegenerative diseases. Our results indicate that NHR-85 is a functional orthologue of PPAR $\delta$  and support the use of *C. elegans* as a powerful *in vivo* model for dissecting PPAR $\delta$ -related metabolic and neurodegenerative processes.

**KEY WORDS:**  $\alpha$ -Synuclein, Fat metabolism, Mitochondrial homeostasis, Mitophagy, NHR-85

## INTRODUCTION

Peroxisome proliferator-activated receptors (PPARs) are ligand-activated transcription factors that play a crucial role in the regulation of systemic metabolism. Of the three isoforms – PPAR $\alpha$ , PPAR $\gamma$  and PPAR $\delta$  (also known as PPAR $\beta$ ) – PPAR $\delta$  is predominantly expressed in the brain, particularly in neurons, but also in oligodendrocytes and microglia (Strosznajder et al., 2021). Structurally, PPAR $\delta$  consists of an autonomous transactivation domain (AF-1), a DNA-binding domain and a ligand-binding domain (Montaigne et al., 2021), similar to the other PPAR isoforms. Functionally, PPAR $\delta$  is a key regulator of lipid and glucose metabolism, mediating a metabolic shift from glycolysis to oxidative phosphorylation and modulating the expression of specific target genes in response to environmental stimuli (Magadum and Engel, 2018; Strosznajder et al., 2021). Activation of PPAR $\delta$  by natural ligands, such as polyunsaturated fatty acids (PUFAs) or

synthetic agonists, has been shown to alter brain lipid composition, including regulation of phospholipid content and cholesterol release, thereby contributing to lipid homeostasis (Strosznajder et al., 2021). Despite this knowledge, the precise molecular mechanisms and signalling cascades by which PPAR $\delta$  contributes to the maintenance of lipid homeostasis remain poorly understood.

Over the past years, agonists against PPARs have attracted considerable attention as therapeutic agents for neurodegenerative diseases. Notably, knockdown of PPAR $\delta$  in the brain has been associated with neuronal loss, mitochondrial dysfunction and widespread alterations in target gene expression (Dickey et al., 2016). Conversely, activation of PPAR $\delta$  has been shown to be neuroprotective, mitigating neurodegeneration and mitochondrial damage in a mouse model of Huntington's disease (HD) (Dickey et al., 2016). Among natural PPAR $\delta$  ligands, the  $\omega$ 9 fatty acid, erucic acid, has emerged as candidate for further investigation in animal models of HD (Altinoz et al., 2020). These findings suggest that PPAR $\delta$  activation might be a viable strategy to address mitochondrial dysfunction and neuronal loss in the context of disease.

*Caenorhabditis elegans* is an ideal and genetically tractable model to study fat and energy regulation by PPAR $\delta$ , as the mammalian pathways of lipid metabolism are conserved in the nematode (Lemieux and Ashrafi, 2015). However, the orthologue of PPAR $\delta$  in *C. elegans* remains uncharacterised. Here, we identify the nematode NHR-85 as a putative orthologue of PPAR $\delta$ . Functional characterisation of this nuclear hormone receptor shows that it regulates both fat and energy metabolism. In addition, we find that NHR-85 exerts a protective effect against  $\alpha$ -synuclein aggregation in a nematode model of Parkinson's disease (PD), through its essential role in mitochondrial homeostasis.

## RESULTS AND DISCUSSION

### NHR-85 is a putative orthologue of PPAR $\delta$

In this study, we sought to identify the *C. elegans* orthologue of human PPAR $\delta$ . We first performed a BLASTp analysis, using the human PPAR $\delta$  protein sequence (NCBI ID: Q03181.1) against the *C. elegans* proteome, which identified NHR-85 as the top candidate protein (query cover 53%, e-value=4e-34). However, a reverse BLASTp search, using the NHR-85 protein sequence (NCBI ID: Q9XUK7.2) against the human proteome, ranked PPAR $\delta$  only as the fifteenth hit (query cover 8%, e-value=2e-33). To assess the validity of the initial BLASTp, we performed a multiple sequence alignment using CLUSTAL (Fig. S1A). We found that the sequences of PPAR $\delta$  and NHR-85 share a high percentage of identical or functionally similar amino acids, suggesting that they have similar roles. We also performed a motif alignment for both proteins to identify whether their annotated domains are functionally conserved (Fig. S1B). Alignment of the zinc-finger domain (zf-C4) revealed a low e-value for both proteins, indicating that the match between the query proteins and the motif is

<sup>1</sup>Institute of Molecular Biology and Biotechnology, Foundation for Research and Technology-Hellas, Heraklion 70013, Crete, Greece. <sup>2</sup>Division of Basic Sciences, School of Medicine, University of Crete, Heraklion 71003, Crete, Greece.

\*Author for correspondence (tavernarakis@imbb.forth.gr)

 N.T., 0000-0002-5253-1466

Handling Editor: Heidi McBride  
Received 29 October 2024; Accepted 2 April 2025

statistically significant. However, for the ligand-binding domain, the *e*-value was low only for PPAR $\delta$ , whereas for NHR-85 it was higher than 0.01 (not significant). Thus, the DNA-binding domain appears to be conserved, suggesting that its function is the same or similar between the two proteins, but the ligand-binding domain has either evolved to lose its functional role or has acquired different binding specificities in *C. elegans*. It is worth noting that orthology does not necessarily imply complete conservation of domain architecture (Koonin et al., 2000, 2004). To identify further functional and evolutionary relationships between the two proteins, we also performed FATCAT flexible alignment (Fig. S2A) which showed that PPAR $\delta$  and NHR-85 are significantly similar ( $P$ -value=3.94e-07, raw FATCAT score=652.89). The chaining result from the alignment revealed 425 equivalent positions with an RMSD of 6.98Å (1 Å=0.1 nm) and four twists (Fig. S2B), and alignment of their structures in 3D (Fig. S2C) suggested that the folding of the two proteins is highly and significantly similar. Finally, we created a phylogenetic tree (Fig. S2D) to place NHR-85 and PPAR $\delta$  in an evolutionary framework. The tree suggests an evolutionary common ancestor that then diverged into vertebrates and invertebrates, with vertebrate sequences clustering together at a relatively higher internal resolution compared to invertebrates, reflecting greater complexity and isoform diversity.

NHR-85 is one of 284 NHRs in *C. elegans*, many of which are known to be involved in fat metabolism (Ashrafi et al., 2003; Liang et al., 2010). Despite the functional roles of other NHRs in metabolic regulation, NHR-85 remains largely unexplored in this

context. Recent studies have provided the first insights into NHR-85 function, revealing its role in regulating the timing and dosage of gene expression during larval development, particularly for the temporal regulation of the microRNA *lin-4*, in co-operation with NHR-23 (Kinney et al., 2023; Myles et al., 2023). This emerging evidence highlights the potential for NHR-85 to have broader biological roles and warrants further investigation to elucidate its functions and mechanisms that govern them.

### Depletion of *nhr-85* affects food intake and neutral lipid accumulation

Previous studies have demonstrated that the expression of *nhr-85* is enhanced upon calorie restriction and is required for mediating stress signals in *C. elegans* during metabolic stress (Ludewig et al., 2014). We examined food intake in *nhr-85(ok2051)* mutants to assess possible changes compared to wild-type (N2) animals. We fed 1-day-old adult animals with HT115 bacteria expressing an isopropylthiogalactoside (IPTG)-inducible monomeric red fluorescent protein (mRFP) (Fig. 1A) and found that *nhr-85(ok2051)* mutants exhibited significantly increased food intake compared to age-matched wild-type worms (Fig. 1B). To confirm this finding, we also assessed pharyngeal pumping in 1-day-old adult wild-type animals treated with control or *nhr-85* RNAi, after validating the efficiency of the RNAi construct (Fig. S3A). Indeed, downregulation of *nhr-85* increased pharyngeal pumping (Fig. S3B). We next investigated whether the elevated food intake led to increased lipid accumulation. To test this, we performed Oil Red O staining,

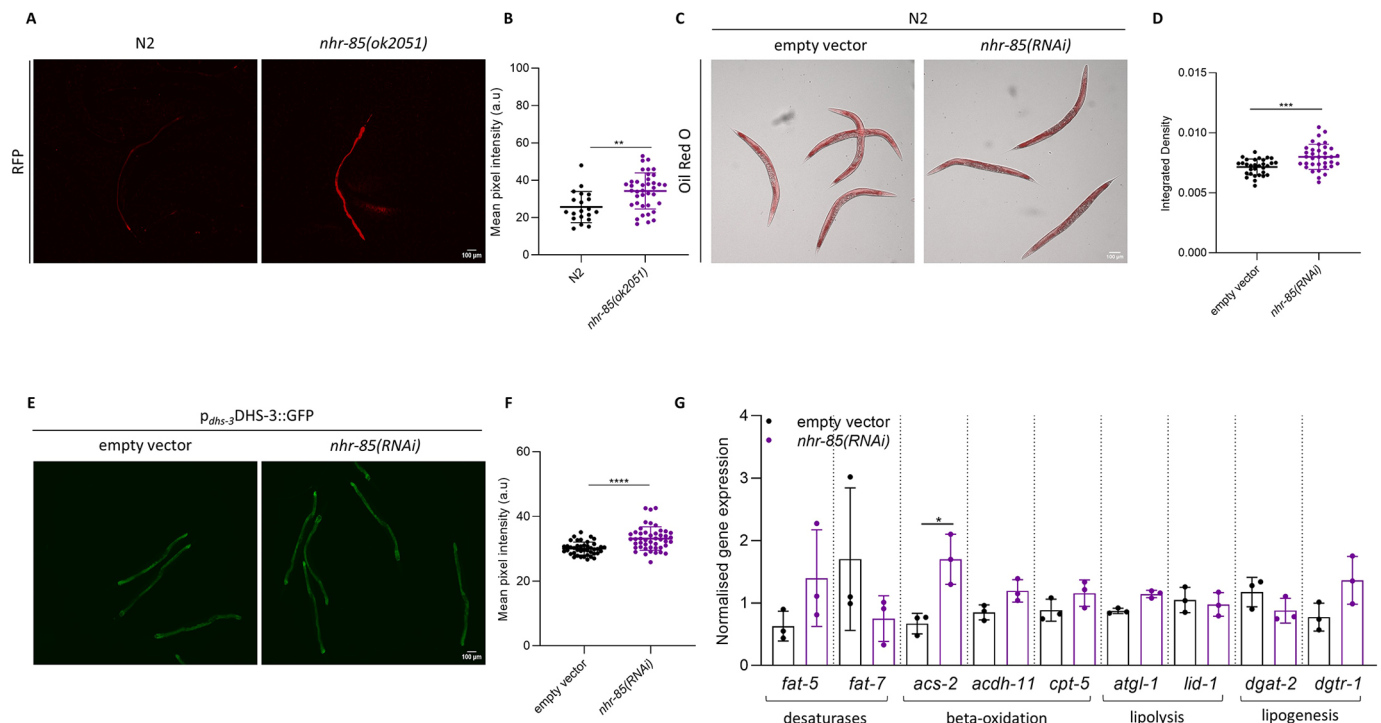


**Fig. 1. NHR-85 regulates food intake and neutral lipid accumulation.** (A) Representative images of wild-type (N2) and *nhr-85(ok2051)* mutants fed with mRFP bacteria. Images were acquired using a 4 $\times$  objective lens. (B) Quantification of the mean pixel intensity of mRFP as shown in A ( $n=40$  animals in total). \*\* $P<0.01$  (two-tailed unpaired *t*-test). (C) Representative images of wild-type (N2) animals treated with empty vector or *nhr-85* RNAi and stained with Oil Red O. Images were acquired using a 4 $\times$  objective lens. (D) Quantification of integrated density in the Oil Red O staining as shown in C ( $n=90$  animals in total). \*\*\* $P<0.001$  (two-tailed unpaired *t*-test). (E) Representative images of transgenic *p<sub>Dhs-3</sub>::DHS-3::GFP* animals treated with empty vector or *nhr-85* RNAi showing intestinal lipid droplets. Images were acquired using a 4 $\times$  objective lens. (F) Quantification of the mean pixel intensity as shown in E ( $n=120$  animals in total). \*\*\*\* $P<0.0001$  (Mann–Whitney unpaired test). (G) Expression analysis of the desaturase genes *fat-5* and *fat-7*, the  $\beta$ -oxidation genes *acs-2*, *acd-11* and *cpt-5*, the lipolysis genes *atgl-1* and *lid-1* and the lipogenesis genes *dgat-2* and *dgtr-1* by RT-qPCR in wild-type (N2) animals treated with empty vector or *nhr-85* RNAi ( $n=3$  independent experiments). \* $P<0.05$  (two-tailed unpaired *t*-test). All error bars show mean $\pm$ s.d. a.u., arbitrary units.

which labels neutral lipids, on wild-type animals treated with control or *nhr-85* RNAi (Fig. 1C). Quantification of the Oil Red O staining revealed a significant increase in neutral lipid accumulation in animals treated with *nhr-85* RNAi compared to control (Fig. 1D). Taken together, these results show that downregulation of *nhr-85* increases food intake, leading to an increase in neutral lipids.

This finding was further supported by using transgenic animals expressing the intestinal lipid droplet membrane protein dehydrogenase-3 (DHS-3) fused to GFP (Na et al., 2015) (Fig. 1E). Quantification of GFP fluorescence intensity in DHS-3::GFP animals showed a marked increase in animals treated with *nhr-85* RNAi compared to controls (Fig. 1F). To explore the potential mechanisms underlying this lipid accumulation, we quantified the expression of key genes involved in fatty acid desaturation,  $\beta$ -oxidation, lipolysis and lipogenesis in animals treated with control or *nhr-85* RNAi (Fig. 1G). No significant differences were observed between the groups, except for the acyl-CoA synthetase gene (*acs-2*), which was significantly upregulated in *nhr-85* RNAi-treated animals (Fig. 1G). This upregulation is likely a compensatory response to the increased fat storage phenotype as well as the high food intake of NHR-85-depleted animals, as ACS-2 is a key enzyme in lipid metabolism that appears to promote the utilization of stored fat in response to the energy requirements of the animals (Van Gilst et al., 2005). Given that *acs-2* encodes a mitochondrial acyl-CoA synthetase involved in fatty acid  $\beta$ -oxidation, we next sought to investigate whether NHR-85 plays a role in regulating mitochondrial abundance and function.

### NHR-85 might modulate mitochondrial mass and function through mitophagy

We assessed the effect of *nhr-85* knockdown on mitochondrial mass, using a body wall muscle (BWM) mitochondrial marker (Fig. 2A). Downregulation of *nhr-85* significantly increased mitochondrial mass in 1-day-old adult animals expressing mitochondria-targeted GFP in BWM compared to age-matched controls (Fig. 2B), suggesting that NHR-85 has a role in balancing mitochondrial content. We also employed super resolution confocal microscopy to assess mitochondrial morphology upon downregulation of *nhr-85* (Fig. 2C) and observed that genetic inhibition of *nhr-85* resulted in mitochondrial network disruption and mitochondrial fragmentation (Fig. 2C,D). To determine whether NHR-85 also affects mitochondrial function, we stained 1-day-old adult wild-type animals treated with control or *nhr-85* RNAi with tetramethylrhodamine, ethyl ester (TMRE), a dye that accumulates only in functional mitochondria due to their negative membrane potential (Fig. 2E). Downregulation of *nhr-85* resulted in decreased TMRE accumulation, as measured by fluorescence intensity, suggesting mitochondrial dysfunction (Fig. 2F). To further assess mitochondrial function, we stained 1-day-old adult wild-type animals with Mitotracker CMXROS (Fig. 2G). As expected, mitochondrial reactive oxygen species (ROS) levels were significantly elevated in *nhr-85* RNAi-treated animals compared to those seen in controls, confirming that mitochondrial dysfunction is associated with *nhr-85* depletion (Fig. 2H).

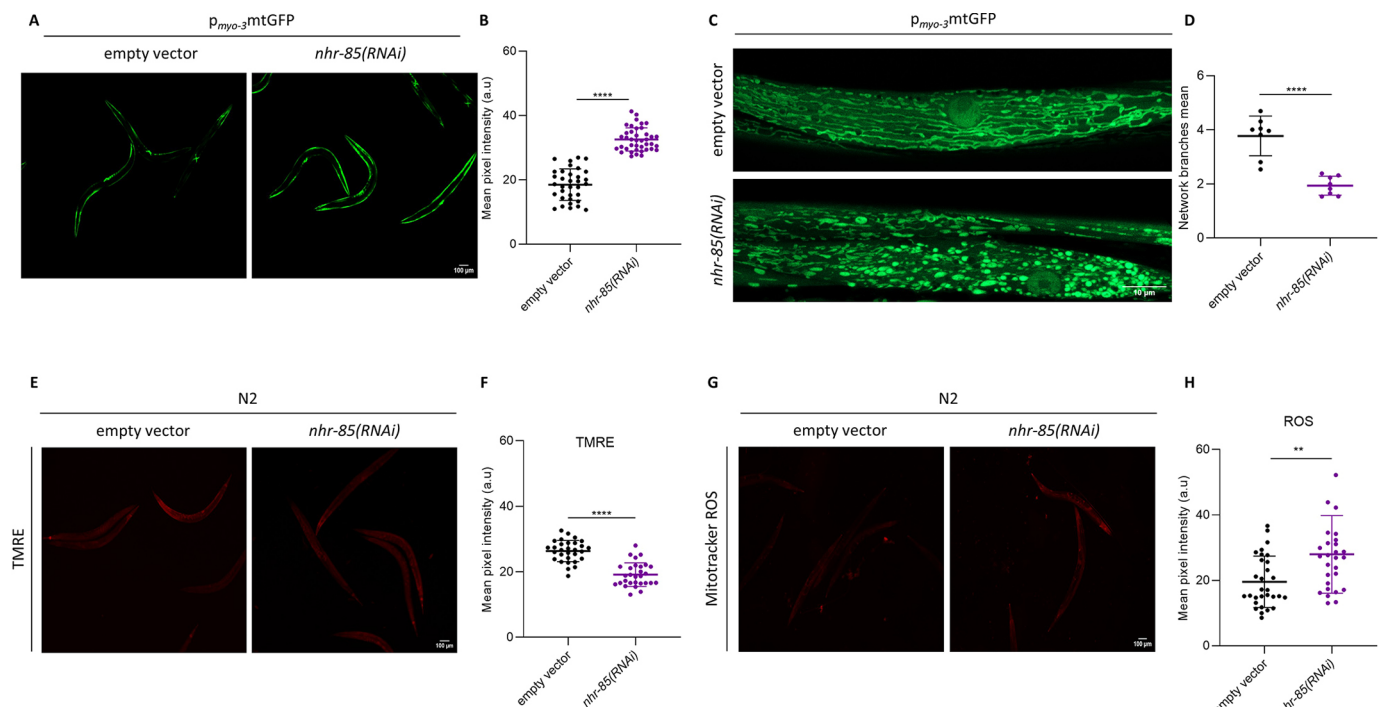


**Fig. 2. Downregulation of *nhr-85* leads to accumulation of dysfunctional mitochondria.** (A) Representative images of transgenic animals expressing p<sub>myo-3</sub>mtGFP after treatment with empty vector or *nhr-85* RNAi showing GFP-tagged mitochondria in BWM cells. Images were acquired using a 4× objective lens. (B) Quantification of the mean pixel intensity of GFP-tagged mitochondria as shown in A ( $n=90$  animals in total). \*\*\*\* $P<0.0001$  (two-tailed unpaired  $t$ -test). (C) Representative confocal images of transgenic animals expressing p<sub>myo-3</sub>mtGFP after treatment with empty vector or *nhr-85* RNAi showing GFP-tagged mitochondria in BWM cells. Images were acquired using a ×40 objective lens. (D) Quantification of the mean mitochondrial network branches as shown in C ( $n=24$  animals in total). \*\*\*\* $P<0.0001$  (two-tailed unpaired  $t$ -test). (E) Representative images of wild-type (N2) animals treated with empty vector or *nhr-85* RNAi and stained with TMRE. Images were acquired using a 4× objective lens. (F) Quantification of the mean pixel intensity of TMRE as shown in E ( $n=90$  animals in total). \*\*\*\* $P<0.0001$  (two-tailed unpaired  $t$ -test). (G) Representative images of wild-type (N2) animals treated with empty vector or *nhr-85* RNAi and stained with Mitotracker Red CM-H2X ROS (images were acquired using a 4× objective lens). Quantification of the mean pixel intensity of Mitotracker Red CM-H2X ROS as shown in G ( $n=90$  animals in total) \*\* $P<0.01$  (Mann–Whitney test). All error bars show mean±s.d. a.u., arbitrary units.

To gain insight into the mechanisms mediating the accumulation of dysfunctional mitochondria upon *nhr-85* downregulation, we used the mitochondria-targeted Rosella (mtRosella) biosensor to monitor mitophagy *in vivo* (Palikaras et al., 2015). We treated animals expressing mtRosella in BWM cells with control or *nhr-85* RNAi and quantified mitophagy during ageing. At day 1 of adulthood, we did not detect any change in mitophagy between treated and untreated animals (Fig. 3A; Fig. S4A), although we detected changes in the expression of certain mitophagy genes upon downregulation of *nhr-85* (Fig. S4B). Interestingly, further temporal analysis revealed a significant reduction in mitophagy in *nhr-85* RNAi-treated animals compared to controls at day 3 (Fig. 3A; Fig. S4C) and day 7 of adulthood (Fig. 3A; Fig. S4D). To confirm these findings, we also treated transgenic animals expressing GFP-tagged mitochondria and the autophagosome marker LGG-1 fused to DsRed in the BWM with control or *nhr-85* RNAi. Increased colocalization indicated the induction of mitophagy. Consistent with the mtRosella results, there was no induction of mitophagy at day 1 of adulthood (Fig. 3B,C), whereas there were fewer colocalization events in animals treated with *nhr-85* RNAi compared to empty vector at both day 3 and day 7 of adulthood (Fig. 3B,C). Thus, NHR-85 is important for maintaining a healthy mitochondrial population, as its downregulation leads to early

mitochondrial dysfunction and failure of mitophagy, which becomes more severe as the organism ages.

### NHR-85 exerts a protective effect against $\alpha$ -synuclein aggregation

Accumulation of dysfunctional mitochondria and impaired mitophagy are well-established pathophysiological features of several neurodegenerative diseases, such as PD, Alzheimer's disease (AD) and HD (Dickey et al., 2016; Fang et al., 2019; Mor et al., 2020). To investigate whether NHR-85 plays a role in  $\alpha$ -synuclein aggregation, we used fluorescence microscopy to analyse a transgenic nematode strain overexpressing  $\alpha$ -synuclein in the BWM, after treatment with control or *nhr-85* RNAi (Fig. 4A). We observed a significant increase in the accumulation of  $\alpha$ -synuclein aggregates with age, upon *nhr-85* downregulation, suggesting that NHR-85 might play a protective role against  $\alpha$ -synuclein toxicity (Fig. 4B). Previous work has shown that aggregated  $\alpha$ -synuclein inhibits mitochondrial function, resulting in decreased adenosine triphosphate (ATP) production and increased ROS generation in neurons (Reeve et al., 2015). Consistent with this, we found increased mitochondrial ROS production with age in transgenic animals overexpressing  $\alpha$ -synuclein in BWM cells after staining with

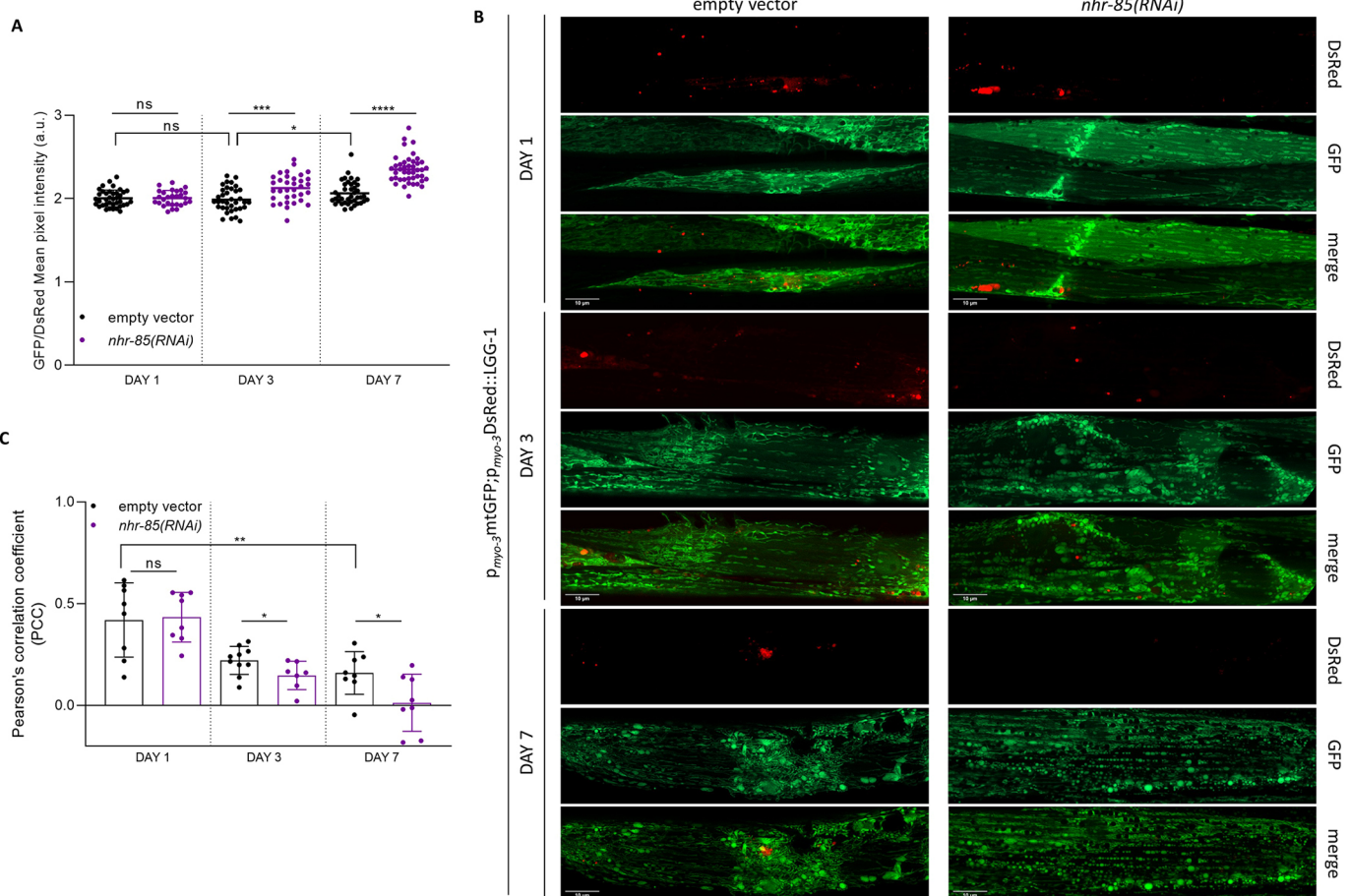


**Fig. 3. NHR-85 is required for the maintenance of mitophagy during ageing.** (A) Quantification of the ratio of pH-sensitive GFP to pH-insensitive DsRed in empty vector and *nhr-85* RNAi-treated animals, at day 1, 3 and 7 of adulthood. Mitophagy stimulation is indicated by a decrease in the GFP/DsRed ratio ( $n=90$  animals in total for each age). \* $P<0.05$ , \*\*\* $P<0.001$ , \*\*\*\* $P<0.0001$  (Mann–Whitney unpaired test). (B) Representative confocal images of transgenic animals expressing a mitochondria-targeted GFP together with the autophagosomal marker LGG-1 fused to DsRed in BWM cells at day 1, 3 and 7 of adulthood after treatment with empty vector or *nhr-85* RNAi. Images were acquired using a 40 $\times$  objective lens. (C) Quantification of the Pearson's correlation coefficient (PCC) values after measuring colocalization events between mitochondria (GFP) and lysosomes (DsRed) in transgenic animals shown in B. Mitophagy stimulation is indicated by increased PCC values ( $n=25$  animals in total for each age). \* $P<0.05$ , \*\* $P<0.01$  (two-tailed unpaired  $t$ -test). All error bars show mean $\pm$ s.d. a.u., arbitrary units.

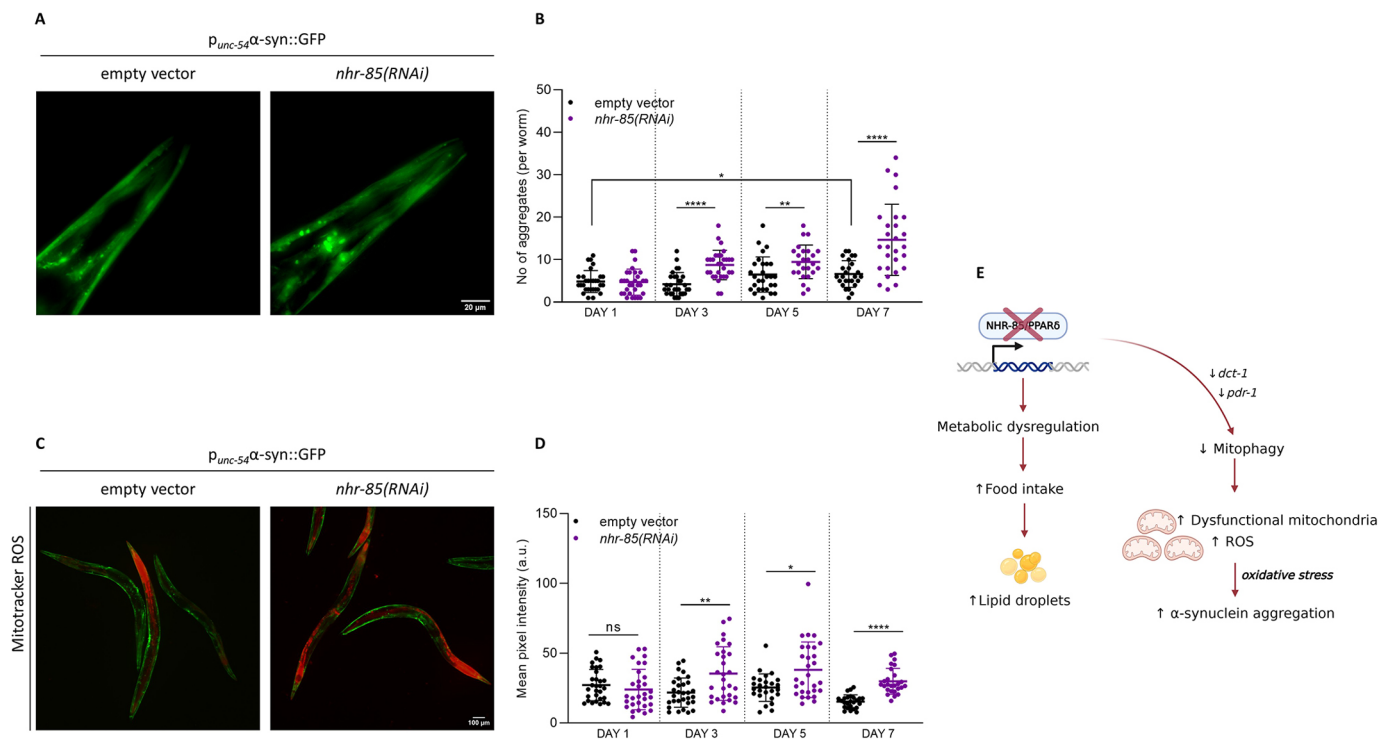


**Fig. 4. NHR-85 shows a protective effect against  $\alpha$ -synuclein aggregation and ROS accumulation in a Parkinson's disease model.**

(A) Representative images of 7-day-old adults expressing GFP-tagged  $\alpha$ -synuclein in BWM cells upon treatment with empty vector or *nhr-85* RNAi. Images were acquired using a 40 $\times$  objective lens. (B) Quantification of the number of aggregates in the head of each worm in empty vector and *nhr-85* RNAi-treated animals at day 1, 3, 5 and 7 of adulthood ( $n=90$  animals in total). \* $P<0.05$ ; \*\* $P<0.01$ ; \*\*\*\* $P<0.0001$  (two-tailed unpaired *t*-test). (C) Representative images of 7-day-old adults expressing GFP-tagged  $\alpha$ -synuclein in BWM cells treated with empty vector or *nhr-85* RNAi and stained with Mitotracker Red CM-H2X ROS. Images were acquired using a 4 $\times$  objective lens. (D) Quantification of the mean pixel intensity of Mitotracker Red CM-H2X ROS in empty vector and *nhr-85* RNAi-treated animals at day 1, 3, 5 and 7 of adulthood ( $n=60$  animals in total). \* $P<0.05$ , \*\* $P<0.01$ , \*\*\*\* $P<0.0001$  (Mann–Whitney test). All error bars show mean $\pm$ s.d. a.u., arbitrary units. (E) Schematic of the proposed model of how NHR-85 affects systemic metabolism and  $\alpha$ -synuclein aggregation. Downregulation of *nhr-85* leads to a metabolic dysregulation, increased food intake and accumulation of lipid droplets. It also decreases mitophagy with age and leads to changes in the expression of certain mitophagy genes such as *dct-1* and *pdr-1*, resulting in the accumulation of dysfunctional mitochondria and increased production of ROS. Conversely, the protective role of NHR-85 against  $\alpha$ -synuclein aggregation might be due, at least in part, to the maintenance of mitophagy. Created in BioRender by Tavernarakis, N., 2025. <https://BioRender.com/j53z222>. This figure was sublicensed under CC-BY 4.0 terms.

Mitotracker ROS (Fig. 4C,D). Interestingly, knockdown of *nhr-85* resulted in a marked further increase in ROS production at day 7 of adulthood (Fig. 4C,D), which could well be related to the significantly increased aggregation of  $\alpha$ -synuclein at this age (Fig. 4A).

In conclusion, our findings indicate that NHR-85 is a putative orthologue of PPAR $\delta$ , although further experimental validation is required to strengthen this orthology. Functionally, NHR-85, akin to PPAR $\delta$ , appears to regulate fundamental biological processes, such as food intake, fat accumulation and energy metabolism. Notably, our results also demonstrate a protective role of NHR-85 against  $\alpha$ -synuclein aggregation, as *nhr-85* downregulation increases the number of aggregates and leads to accumulation of dysfunctional mitochondria and increased ROS generation in a PD nematode model of  $\alpha$ -synuclein, at least in part due to impaired mitophagy (Fig. 4E). Future research should aim to elucidate the specific mechanisms by which NHR-85 mediates neuroprotection in other PD models, potentially providing new insights into early intervention strategies against this neurodegenerative disease.

## MATERIALS AND METHODS

### *C. elegans* strains

Standard procedures were followed for maintaining *C. elegans* strains. All the animals were maintained at 20°C and grown on nematode growth medium plates seeded with OP50 *Escherichia coli* (a uracil-requiring *E. coli* strain derived from *E. coli* strain B; Brenner, 1974; Couillault and Ewbank, 2002).

The following strains used in this study are available from the *Caenorhabditis* Genetics Center (CGC): N2, wild-type Bristol isolate; RB1661, *nhr-85(ok2051)*, *eat-2(ad465)*; LIU1, *ldr1s1* [*p<sub>dhs-3</sub>::DHS-3::GFP + unc-76(+)*]; and SJ4103: N2; *Is*[*p<sub>myo-3</sub>::mtGFP*]. The strain UA49, *baln12* [*p<sub>unc-54</sub>::syn::GFP+rol-6(su1006)*] was generously provided by Guy Cardwell (Department of Biological Sciences, University of Alabama, Alabama, USA), the strain IR253: *unc-119(ed3)*; *Ex*[*p<sub>myo-3</sub>::mtRosella*; *unc-119(+)*] was generously provided by Konstantinos Palikaras (IMBB-FORTH, Greece) and the strain *p<sub>myo-3</sub>::mtGFP*; *p<sub>myo-3</sub>::DsRed::LGG-1* was generously provided by Nikos Champilas (IMBB-FORTH, Greece).

### Food intake

To measure food intake, we fed synchronized animals on day 1 of adulthood with HT115 bacteria transformed with an isopropylthiogalactoside (IPTG)-inducible RFP-expressing plasmid for 5 min, as described previously (Champilas et al., 2020). The experiment was repeated twice. For each experiment, 20 animals were examined per condition. Pharyngeal pumping was measured as previously described (Champilas et al., 2020). Briefly, grinder movements of free-moving animals were measured under the stereoscope in three independent experiments and the number of pumps per animal was recorded using a clicker. For each experiment, 20 animals were examined per condition.

### RNA interference and molecular cloning

For gene knockdown by RNAi, we used HT115 (DE3) *E. coli* bacteria transformed with the L4440 plasmid vector expressing double-stranded RNA against the gene of interest. As a control, we used the empty vector

L4440. The *nhr-85* RNAi construct was generated by PCR amplification of a gene-specific region using *C. elegans* genomic DNA as a template and the following primer sets: 5'-GTGCCAAAACGTGAGAAAGC-3' and 5'-TGCTCATCAGAATCCACGTC-3'. The resulting construct was then inserted into the TOPO-pCRII vector (Invitrogen) by TA cloning and subcloned into the final L4440 vector at the BamHI/AvaI sites. Positive clones were transformed into HT115 bacteria to allow knockdown through feeding (Fire et al., 1998). For each RNAi experiment, a single bacterial colony was inoculated into LB medium (10 g Bacto-tryptone, 5 g Bacto-yeast extract, 10 g NaCl, H<sub>2</sub>O to 1 l, pH 7.0) containing 100 µg/ml ampicillin (AppliChem IWM Reagents, A0839) and 10 µg/ml tetracycline (AppliChem IWM Reagents, A2228) overnight at 37°C on a shaker with 150 rpm for 16 h. Thereafter, 250 µl of overnight culture were inoculated in LB medium containing 100 µg/ml ampicillin for 3–4 h, and RNAi plates were seeded with 250 µl of bacterial culture containing IPTG (Apollo Scientific, BIMB1008) at a final concentration of 2 mM.

#### mRNA quantification and qPCR

To quantify gene expression, total RNA was extracted using the TRIzol reagent (Invitrogen) from wild-type animals treated with empty vector or *nhr-85* RNAi. All the primers used are summarized in Table S1, and *actin-1* was used as the housekeeping gene. For cDNA synthesis, mRNA was reverse transcribed using an iScript™ cDNA Synthesis Kit (Bio-Rad). Quantitative (q)PCR was performed in triplicate with the Eva Green qPCR Kit (Biotium) in a Bio-Rad CFX96 Real-Time PCR system (Bio-Rad), according to the manufacturer's instructions. For each experiment, 150 animals were used for RNA extraction per condition.

#### Oil Red O staining

To assess fat accumulation, synchronized animals at day one of adulthood were stained with Oil Red O, which stains only neutral lipids (O'Rourke et al., 2009). Briefly, for each experiment, 100 worms (for each condition) were washed three times with M9 (3 g KH<sub>2</sub>PO<sub>4</sub>, 6 g Na<sub>2</sub>HPO<sub>4</sub>, 5 g NaCl, 1 ml 1 M MgSO<sub>4</sub>, H<sub>2</sub>O to 1 l) and allowed to settle at the bottom of the tube. The supernatant was removed, and worms were fixed with 1% paraformaldehyde (PFA), dissolved in M9 at a 1:1 ratio. The samples were rotated for 30 min at room temperature and then freeze-thawed three times in an ethanol-dry ice bath. Animals were allowed to settle by gravity and washed three times with M9 to remove PFA. The worms were then resuspended in 60% isopropanol and incubated for 15 min at room temperature. After the worms were allowed to settle, the isopropanol was removed, 1 ml of 60% Oil Red O stain was added, and the animals were incubated at room temperature for 4 h. The stain was removed by washing three times with M9. Animals were mounted and imaged using an EVOS FL Auto 2 imaging system (AMAFD2000; Thermo Fisher Scientific). The experiment was repeated at least three times.

#### TMRE staining

To assess mitochondrial function, we stained synchronized 1-day-old adult animals with TMRE (a dye that accumulates in intact mitochondria; Molecular Probes, Invitrogen, T669). For each experiment, 30 animals per condition were transferred at the L4 stage to plates containing heat-inactivated RNAi bacteria (UV, 15 min) and 100 µl of TMRE at a final concentration of 0.05 µM. Animals were incubated overnight at 20°C before immobilization with levamisole (Sigma-Aldrich, 196142) and mounting for microscopic examination using an EVOS FL Auto 2 imaging system (AMAFD2000; Thermo Fisher Scientific). The experiment was repeated at least three times.

#### MitoTracker CM-H2X ROS staining

To assess ROS production, we stained synchronized 1-day-old adult animals with MitoTracker Red CM-H2X ROS (Molecular Probes, Invitrogen, M7513). For each experiment, 30 animals per condition were transferred at the L4 stage on plates with heat-inactivated RNAi bacteria (UV, 15 min) and 100 µl of MitoTracker Red CM-H2X ROS, a dye that is highly sensitive to alterations in mitochondrial membrane potential, at a final concentration of 0.1 µM. Animals were incubated overnight at 20°C before immobilization with levamisole and mounting for microscopic examination using an EVOS FL Auto 2 imaging system (AMAFD2000; Thermo Fisher Scientific). The experiment was repeated at least three times.

#### Imaging

For live imaging, we used synchronized transgenic animals such as *p<sub>myo-3</sub>-mtGFP*, carrying the indicated somatic fluorescence reporters. Briefly, worms were paralyzed on microscope slides with 20 mM levamisole and mounted. Microscopic examination of all worms was performed using an EVOS FL Auto 2 imaging system (AMAFD2000; Thermo Fisher Scientific). The mean pixel intensity or the number of particles was then calculated for each animal using the ImageJ software. For each experiment, at least 30 animals were examined per condition and each experiment was repeated at least three times.

#### Mitochondrial imaging

To analyse the mitochondrial network, we employed super resolution confocal imaging with ZEISS LSM 900 with Airyscan and acquired z-stack images using a 40× objective lens for the SJ4103 strain. We then used the ImageJ plugin MINA (<https://imagej.net/plugins/mina>) to analyse the mitochondrial branches of the network. All images were processed with the same settings: median filter at a radius of 1 pixel, Contrast Limited Adaptive Histogram Equalization (CLAHE) with block size at 10 and histogram Bins at 256 and otsu thresholding for consistent and robust segmentation. In each experiment, ten animals were examined per condition and each experiment was repeated at least three times.

#### Mitophagy monitoring

To monitor mitophagy, we used the reporter *p<sub>myo-3</sub>mtRosella*, which expresses a dual fluorescent probe composed of a pH-sensitive GFP and a pH-insensitive DsRed protein (Palikaras et al., 2019). Mitophagy activity events were calculated as the ratio between the number of pixels of GFP and DsRed (GFP/DsRed). Thus, a reduction in the ratio correlates with increased mitophagy. For each experiment, 30 animals were examined per condition for each age and each experiment was repeated at least three times. Moreover, we employed super resolution confocal microscopy with ZEISS LSM 900 with Airyscan and acquired z-stack images with a 40× objective lens on transgenic animals expressing a mitochondria-targeted GFP, together with the autophagosomal marker LGG-1 fused with DsRed in BWM cells. Mitophagy stimulation is indicated as increased colocalization events. For each experiment, at least eight animals were examined per condition at each age and each experiment was repeated at least three times.

#### Statistical analysis

We used the Prism software package (GraphPad Software 8) for statistical analysis. The statistical tests applied for each experiment are specified in the figure legends.

#### Acknowledgements

We thank the *Caenorhabditis* Genetics Center (CGC), which is funded by the NIH Office of Research Infrastructure Programs (P40 OD010440), for providing the nematode strains used here.

#### Competing interests

The authors declare no competing or financial interests.

#### Author contributions

Conceptualization: D.T., M.M., N.T.; Formal analysis: D.T.; Funding acquisition: N.T.; Investigation: D.T., M.M., N.T.; Methodology: D.T., M.M., N.T.; Resources: D.T., M.M., N.T.; Supervision: M.M., N.T.; Validation: D.T., N.T.; Visualization: D.T., N.T.; Writing – original draft: D.T., M.M.; Writing – review & editing: D.T., M.M., N.T.

#### Funding

Work in the authors' laboratory is funded by the Hellenic Foundation for Research and Innovation (H.F.R.I.) under the '1st Call for H.F.R.I. Research Projects to support Faculty members and Researchers and the procurement of high-cost research equipment' (Project Number: HFRI-FM17C3-0869, NeuroMitophagy), the General Secretariat for Research and Innovation of the Greek Ministry of Development, the European Union – NextGenerationEU (project code: TAEDR-0535850, Acronym: BrainPrecision) in the framework of the Action 'Flagship Actions in Interdisciplinary Scientific Areas with Special Interest in Connection to the Productive Fabric', under the National Recovery and Resilience Plan 'Greece 2.0' and the European Commission Research Executive Agency Excellence Hub 'CHangeing' (GA-101087071). D.T. is supported by the Hellenic Foundation for Research and Innovation (H.F.R.I.) (Scholarship Code: 11403).

**Data and resource availability**

All relevant data can be found within the article and its [supplementary information](#).

**First Person**

This article has an associated First Person interview with the first author of the paper.

**Peer review history**

The peer review history is available online at <https://journals.biologists.com/jcs/lookup/doi/10.1242/jcs.263651.reviewer-comments.pdf>

**Special Issue**

This article is part of the Special Issue 'Cell Biology of Mitochondria', guest edited by Ana J. Garcia-Saez and Heidi McBride. See related articles at <https://journals.biologists.com/jcs/issue/138/9>.

**References**

- Altinoz, M. A., Ozpınar, A., Ozpınar, A. and Hacker, E.** (2020). Erucic acid, a nutritional PPARdelta-ligand may influence Huntington's disease pathogenesis. *Metab. Brain Dis.* **35**, 1-9. doi:10.1007/s11011-019-00500-6
- Ashrafi, K., Chang, F. Y., Watts, J. L., Fraser, A. G., Kamath, R. S., Ahringer, J. and Ruvkun, G.** (2003). Genome-wide RNAi analysis of *Caenorhabditis elegans* fat regulatory genes. *Nature* **421**, 268-272. doi:10.1038/nature01279
- Brenner, S.** (1974). The genetics of *Caenorhabditis elegans*. *Genetics* **77**, 71-94. doi:10.1093/genetics/77.1.71
- Champilas, N., Ruckenstein, C., Sica, V., Buttner, S., Habernig, L., Dichtinger, S., Madeo, F., Tavernarakis, N., Bravo-San Pedro, J. M. and Kroemer, G.** (2020). Acyl-CoA-binding protein (ACBP): a phylogenetically conserved appetite stimulator. *Cell Death Dis.* **11**, 7. doi:10.1038/s41419-019-2205-x
- Couillault, C. and Ewbank, J. J.** (2002). Diverse bacteria are pathogens of *Caenorhabditis elegans*. *Infect Immun.* **70**, 4705-4707. doi:10.1128/IAI.70.8.4705-4707.2002
- Dickey, A. S., Pineda, V. V., Tsunemi, T., Liu, P. P., Miranda, H. C., Gilmore-Hall, S. K., Lomas, N., Sampat, K. R., Buttgerit, A., Torres, M. J. et al.** (2016). PPARdelta is repressed in Huntington's disease, is required for normal neuronal function and can be targeted therapeutically. *Nat. Med.* **22**, 37-45. doi:10.1038/nm.4003
- Fang, E. F., Hou, Y., Palikaras, K., Adriaanse, B. A., Kerr, J. S., Yang, B., Lautrup, S., Hasan-Olive, M. M., Caponio, D., Dan, X. et al.** (2019). Mitophagy inhibits amyloid-beta and tau pathology and reverses cognitive deficits in models of Alzheimer's disease. *Nat. Neurosci.* **22**, 401-412. doi:10.1038/s41593-018-0332-9
- Fire, A., Xu, S., Montgomery, M. K., Kostas, S. A., Driver, S. E. and Mello, C. C.** (1998). Potent and specific genetic interference by double-stranded RNA in *Caenorhabditis elegans*. *Nature* **391**, 806-811. doi:10.1038/35888
- Kinney, B., Sahu, S., Stec, N., Hills-Muckey, K., Adams, D. W., Wang, J., Jaremko, M., Joshua-Tor, L., Keil, W. and Hammell, C. M.** (2023). A circadian-like gene network programs the timing and dosage of heterochronic miRNA transcription during *C. elegans* development. *Dev. Cell* **58**, 2563-2579. doi:10.1016/j.devcel.2023.08.006
- Koonin, E. V., Aravind, L. and Kondrashov, A. S.** (2000). The impact of comparative genomics on our understanding of evolution. *Cell* **101**, 573-576. doi:10.1016/S0092-8674(00)80867-3
- Koonin, E. V., Fedorova, N. D., Jackson, J. D., Jacobs, A. R., Krylov, D. M., Makarova, K. S., Mazumder, R., Mekhedov, S. L., Nikolskaya, A. N., Rao, B. S. et al.** (2004). A comprehensive evolutionary classification of proteins encoded in complete eukaryotic genomes. *Genome Biol.* **5**, R7. doi:10.1186/gb-2004-5-2-r7
- Lemieux, G. A. and Ashrafi, K.** (2015). Insights and challenges in using *C. elegans* for investigation of fat metabolism. *Crit. Rev. Biochem. Mol. Biol.* **50**, 69-84. doi:10.3109/10409238.2014.959890
- Liang, B., Ferguson, K., Kadyk, L. and Watts, J. L.** (2010). The role of nuclear receptor NHR-64 in fat storage regulation in *Caenorhabditis elegans*. *PLoS ONE* **5**, e9869. doi:10.1371/journal.pone.0009869
- Ludewig, A. H., Klapper, M. and Doring, F.** (2014). Identifying evolutionarily conserved genes in the dietary restriction response using bioinformatics and subsequent testing in *Caenorhabditis elegans*. *Genes Nutr.* **9**, 363. doi:10.1007/s12263-013-0363-5
- Magadum, A. and Engel, F. B.** (2018). PPARbeta/delta: linking metabolism to regeneration. *Int. J. Mol. Sci.* **19**, 2013. doi:10.3390/ijms19072013
- Montaigne, D., Butruille, L. and Staels, B.** (2021). PPAR control of metabolism and cardiovascular functions. *Nat. Rev. Cardiol.* **18**, 809-823. doi:10.1038/s41569-021-00569-6
- Mor, D. E., Sohrabi, S., Kaletsky, R., Keyes, W., Tartici, A., Kalia, V., Miller, G. W. and Murphy, C. T.** (2020). Metformin rescues Parkinson's disease phenotypes caused by hyperactive mitochondria. *Proc. Natl. Acad. Sci. USA* **117**, 26438-26447. doi:10.1073/pnas.2009838117
- Myles, K. M., Clancy, J. C., Johnson, L. C., Ashley, G., Manzano, J., Ragle, J. M. and Ward, J. D.** (2023). An nhr-85::GFP::AID::3xFLAG knock-in allele for investigation of molting and oscillatory gene regulation. *MicroPubl. Biol.* **2023**, 10.17912/micropub.biology.00099. doi:10.17912/micropub.biology.000993
- Na, H., Zhang, P., Chen, Y., Zhu, X., Liu, Y., Liu, Y., Xie, K., Xu, N., Yang, F., Yu, Y. et al.** (2015). Identification of lipid droplet structure-like/resident proteins in *Caenorhabditis elegans*. *Biochim. Biophys. Acta* **1853**, 2481-2491. doi:10.1016/j.bbmr.2015.05.020
- O'Rourke, E. J., Soukas, A. A., Carr, C. E. and Ruvkun, G.** (2009). *C. elegans* major fats are stored in vesicles distinct from lysosome-related organelles. *Cell Metab.* **10**, 430-435. doi:10.1016/j.cmet.2009.10.002
- Palikaras, K., Lionaki, E. and Tavernarakis, N.** (2015). Coordination of mitophagy and mitochondrial biogenesis during ageing in *C. elegans*. *Nature* **521**, 525-528. doi:10.1038/nature14300
- Palikaras, K., Lionaki, E. and Tavernarakis, N.** (2019). Mitophagy dynamics in *Caenorhabditis elegans*. *Methods Mol. Biol.* **1880**, 655-668. doi:10.1007/978-1-4939-8873-0\_43
- Reeve, A. K., Ludtmann, M. H., Angelova, P. R., Simcox, E. M., Horrocks, M. H., Klenerman, D., Gandhi, S., Turnbull, D. M. and Abramov, A. Y.** (2015). Aggregated alpha-synuclein and complex I deficiency: exploration of their relationship in differentiated neurons. *Cell Death Dis.* **6**, e1820. doi:10.1038/cddis.2015.166
- Strosznajder, A. K., Wojtowicz, S., Jezyna, M. J., Sun, G. Y. and Strosznajder, J. B.** (2021). Recent insights on the role of PPAR-beta/delta in neuroinflammation and neurodegeneration, and its potential target for therapy. *Neuromolecular Med.* **23**, 86-98. doi:10.1007/s12017-020-08629-9
- Van Gilst, M. R., Hadjivassiliou, H., Jolly, A. and Yamamoto, K. R.** (2005). Nuclear hormone receptor NHR-49 controls fat consumption and fatty acid composition in *C. elegans*. *PLoS Biol.* **3**, e53. doi:10.1371/journal.pbio.0030053